iScience

CellPress
OPEN ACCESS

Article

Effects of beta-band and gamma-band rhythmic stimulation on motor inhibition

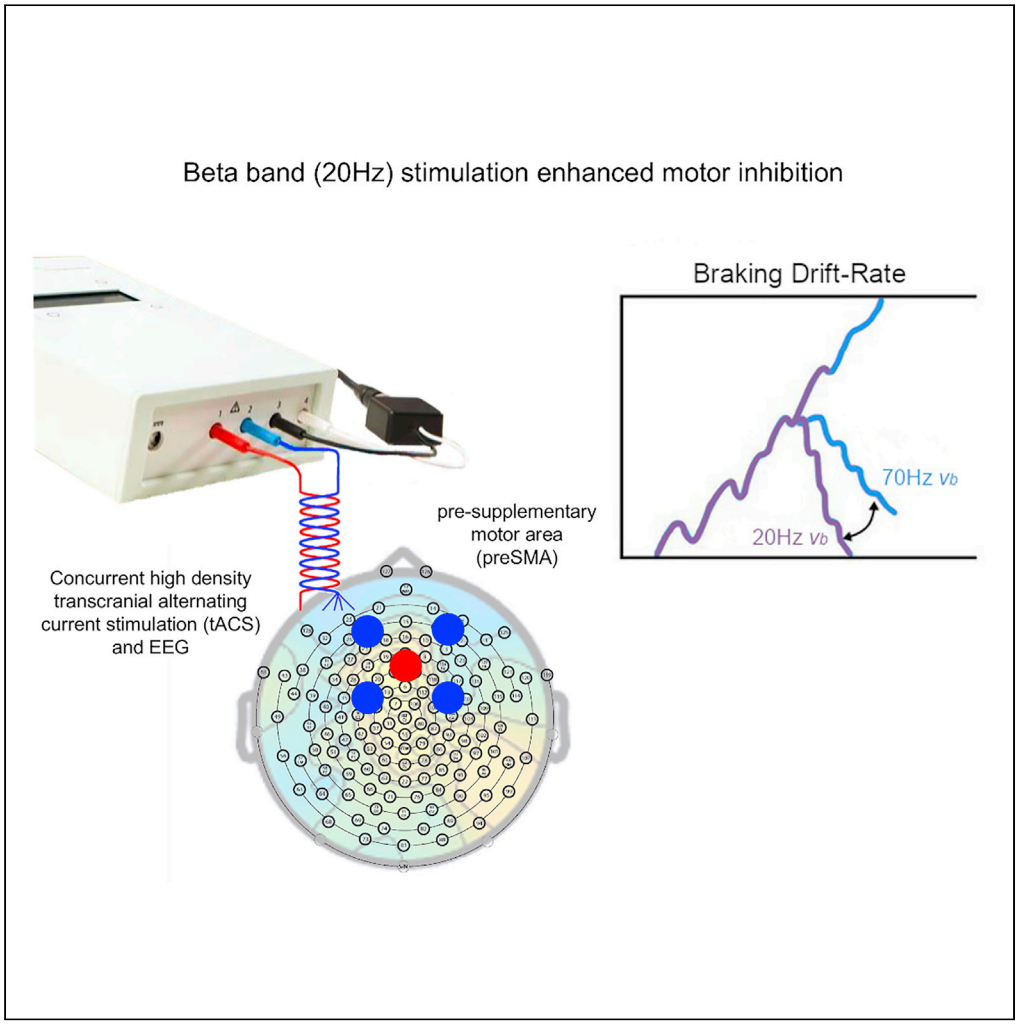

Inge Leunissen, Manon Van Steenkiste, Kirstin-Friederike Heise, ..., Dante Mantini, James P. Coxon, Stephan P. Swinnen

inge.leunissen@maastrichtuniversity.nl

Highlights

Beta tACS over preSMA improved motor inhibition

Gamma tACS slowed down the stop process but primarily affected movement execution

Beta tACS resulted in higher beta spectral power around the time of the stop-signal

Effects of tACS showed a dose-response relationship with electric field strength

Leunissen et al., iScience 25, 104338
May 20, 2022
https://doi.org/10.1016/j.isci.2022.104338

iScience

CellPress
OPEN ACCESS

Article

Effects of beta-band and gamma-band rhythmic stimulation on motor inhibition

Inge Leunissen,[1,2,8,*] Manon Van Steenkiste,[1] Kirstin-Friederike Heise,[1,6] Thiago Santos Monteiro,[1,6] Kyle Dunovan,[3] Dante Mantini,[1,4] James P. Coxon,[5,7] and Stephan P. Swinnen[1,6,7]

SUMMARY

To investigate whether beta oscillations are *causally* related to motor inhibition, thirty-six participants underwent two concurrent transcranial alternating current stimulation (tACS) and electroencephalography (EEG) sessions during which either beta (20 Hz) or gamma (70 Hz) stimulation was applied while participants performed a stop-signal task. In addition, we acquired magnetic resonance images to simulate the electric field during tACS. 20 Hz stimulation targeted at the pre-supplementary motor area enhanced inhibition and increased beta oscillatory power around the time of the stop-signal in trials directly following stimulation. The increase in inhibition on stop trials followed a dose-response relationship with the strength of the individually simulated electric field. Computational modeling revealed that 20 and 70 Hz stimulation had opposite effects on the braking process. These results highlight that the effects of tACS are state-dependent and demonstrate that fronto-central beta activity is causally related to successful motor inhibition, supporting its use as a functional biomarker.

INTRODUCTION

Inhibitory control, such as the ability to suppress an already initiated movement, is essential in everyday life. Successful motor inhibition activates a distributed network of cortical and subcortical areas with the pre-supplementary motor area (preSMA), the right inferior frontal cortex (rIFC), and the subthalamic nucleus (STN), which are identified as key nodes (Aron et al., 2016; Jahanshahi et al., 2015). However, the exact nature of the neural dynamics within this fronto-basal-ganglia network is not entirely clear.

Long-distance neural communication is thought to arise from groups of neurons engaging in rhythmic synchronization (Fries, 2005). In the human motor system, cortical and subcortical gamma-band oscillatory activity (60–100 Hz) increases during voluntary movement (Litvak et al., 2012; Crone et al., 1998), suggesting it has a prokinetic role. In contrast, oscillatory activity in the beta-band (13–30 Hz) is prominent during tonic contractions and decreases before and during movement (Schmidt et al., 2019; Engel and Fries, 2010). Excessive beta oscillations, as in Parkinson's disease, are associated with slowing of movement and rigidity (Kuhn et al., 2004; Little and Brown, 2014). This has led to the idea that beta activity might promote the inhibition of movement.

Indeed, electrophysiological recordings have revealed increased beta oscillations in preSMA, rIFC, and STN during successful motor inhibition (Alegre et al., 2013; Kuhn et al., 2004; Ray et al., 2012; Swann et al., 2009, 2012; Wagner et al., 2018; Wessel et al., 2013, 2016; Castiglione et al., 2019) [for an overview of electrophysiological correlates of inhibitory control see Huster et al., 2017]. Crucially, this activity was seen after the presentation of a stop-signal but before the completion of the stop process (as indexed by the stop-signal reaction time; SSRT). Yet, others reported that beta oscillations primarily increase after the SSRT (Fischer et al., 2017; Jha et al., 2015) or without differentiation between successful and unsuccessful stops (Fonken et al., 2016). These authors suggest that fronto-subthalamic beta activity is not *necessary* for stopping but rather reflects post-processing of the stop-signal trial and is perhaps responsible for the slowing that is typically observed on trials that follow a stop signal (Bissett and Logan, 2012). Thus, controversy exists over the role of beta oscillatory activity in successful inhibition.

[1]Movement Control and Neuroplasticity Research Group, Department of Movement Sciences, Group Biomedical Sciences, KU Leuven, 3000, Leuven, Belgium

[2]Section Brain Stimulation and Cognition, Department of Cognitive Neuroscience, Faculty of Psychology and Neuroscience, Maastricht University, 6200MD, Maastricht, the Netherlands

[3]Department of Psychology and Center for the Neural Basis of Cognition, Carnegie Mellon University, Pittsburgh, PA 15213, USA

[4]Brain Imaging and Neural Dynamics Research Group, IRCCS San Camillo Hospital, 30126, Venice, Italy

[5]School of Psychological Sciences and Turner Institute for Brain and Mental Health, Monash University, Clayton, VIC 3800, Australia

[6]KU Leuven Brain Institute (LBI), KU Leuven, 3000, Leuven, Belgium

[7]Senior author

[8]Lead contact

*Correspondence: inge.leunissen@maastrichtuniversity.nl

https://doi.org/10.1016/j.isci.2022.104338

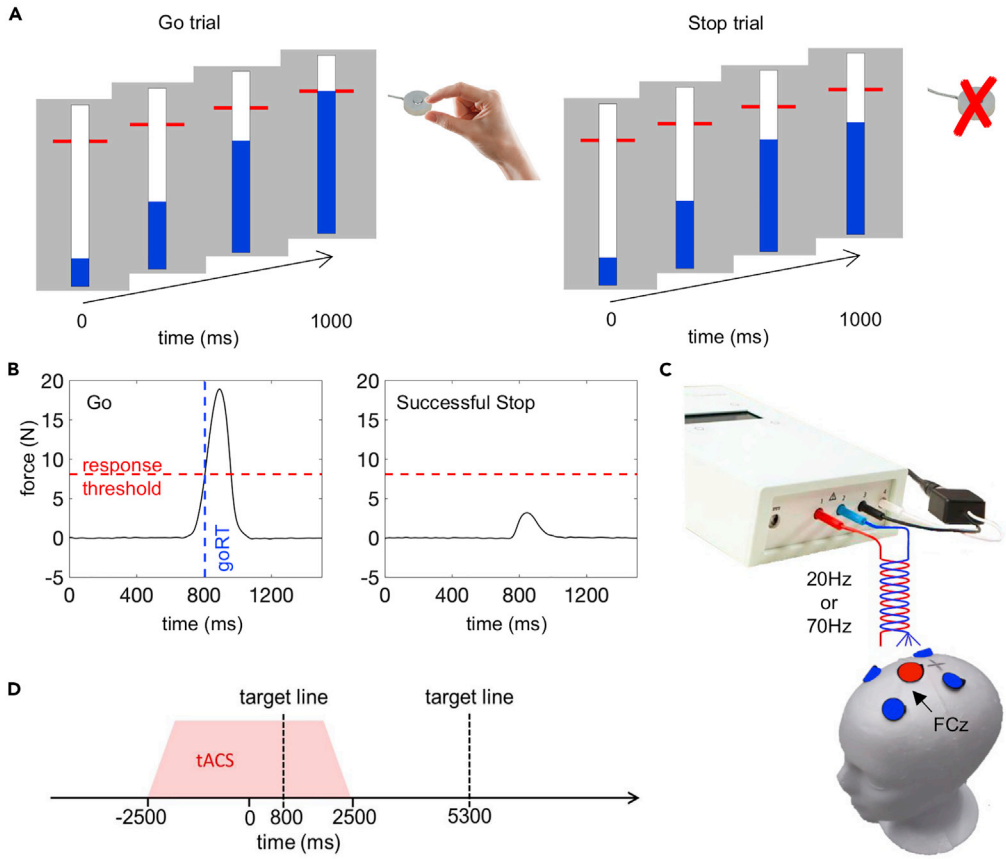

Figure 1. Experimental design

(A) Anticipated response version of stop-signal paradigm. An indicator (depicted in blue) increased from the bottom up at constant velocity reaching the top in 1 s. In 'go' trials, participants had to stop the indicator as close as possible to the red target line by squeezing a force sensor. In 'stop' trials, the bar would stop filling before it reached the target line and participants were instructed to withhold their response.

(B) Example force trace of a go trial and a successful stop with a partial response. Response times were recorded as the time between indicator fill onset and the moment the force signal first exceeded the response threshold (~30% of maximum voluntary force). Stop trials were classified as failed stop trials if the force produced exceeded the response threshold. If the force remained below the threshold, the trial was classified as successfully inhibited.

(C) Electrode montage with center electrode (Ø 2.5cm) over FCz and surrounding electrodes at ~5cm center-to-center distance (Ø 2cm).

(D) Event-related alternating current stimulation ensued randomly in 40% of the trials. Stimulation commenced 2.5s before indicator fill onset and lasted for a total of 5s including fading in/out phase of 0.5s. Between the end of the previous and the start of the next stimulation trains was a minimum interval of 4.5s.

Investigation of causal oscillation-function relationships requires experimental control over the strength and/or phase of the ongoing brain rhythms. This can be achieved with transcranial alternating current stimulation (tACS) (Helfrich et al., 2014; Herrmann et al., 2016; Thut et al., 2011). Gamma-band tACS (70Hz) over the primary motor cortex (M1) increases movement amplitude, force development, and velocity (Guerra et al., 2018; Joundi et al., 2012; Moisa et al., 2016). Whereas, beta-band stimulation (20 Hz) over M1 results in reduced motor output (Guerra et al., 2018; Joundi et al., 2012; Pogosyan et al., 2009; Wach et al., 2013). There is limited evidence that 20 Hz tACS over M1 reduces response force specifically on no-go trials in context of a go/no-go task (Joundi et al., 2012). Here, we made use of a stop-signal task (Figure 1). Importantly, while the go/no-go task most likely indexes action restraint, i.e., the decision to respond or not, stop-signal paradigms allow for investigation of action cancellation, i.e., overriding an already initiated action (Leunissen et al., 2017; Raud et al., 2020). We substantially extend upon previous studies of M1 tACS by instead stimulating one of the key nodes in the putative fronto-basal ganglia network for inhibitory control, the preSMA, for which beta oscillatory dynamics have been related to successful movement cancellation

Table 1. Effect of stimulation on stop-signal task performance

Trial type	20Hz Unstimulated	20Hz Stimulated	70Hz Unstimulated	70Hz Stimulated	LME statistics			
					df, Error df	Main effect of frequency (20Hz, 70Hz)	Main effect of stimulation (ON, OFF)	Interaction
Go								
% early response	0.0	0.0	0.0	0.0	NA	NA	NA	NA
% no response	1.7 ± 2.29	1.57 ± 2.46	1.56 ± 2.24	1.53 ± 2.48	1, 102	F = 0.14 p = 0.705	F = 0.04 p = 0.851	F = 0.16 p = 0.694
goRT (ms)	17.96 ± 43.64	16.90 ± 43.73	18.10 ± 42.4	17.15 ± 42.6	1, 28,138	F = 0.69 p = 0.407	F = 3.71 p = 0.054	F = 0.0 p = 0.968
Stop								
Stop fail RT (ms)	−1.5 ± 34.09	−2.40 ± 34.14	−2.47 ± 33.74	−2.00 ± 33.24	1, 6937	F = 0.27 p = 0.606	F = 0.05 p = 0.818	F = 0.72 p = 0.395
% inhibit	51.26 ± 0.58	51.75 ± 0.69	51.38 ± 0.64	51.78 ± 0.7	1, 102	F = 0.8 p = 0.359	**F = 26.8 p < 0.0001**	F = 0.3 p = 0.611
SSRT (ms)	189.4 ± 12.42	191.1 ± 11.24	193.36 ± 12.22	192.4 ± 12.3	1, 102	**F = 5.36 p = 0.023**	F = 0.1 p = 0.748	F = 1.37 p = 0.244

GoRT and stop fail RT are expressed relative to the target (i.e. response – 800 ms). Mean ± SD is reported. LME = linear mixed model. Results for LME models are given as Type III sums of squares for sequentially fitted fixed effects. Statistically significant findings are highlighted in bold.

(Wessel, 2020). We hypothesized that beta stimulation targeting preSMA will facilitate response inhibition; besides, given the opposing roles of beta and gamma oscillations in the motor system, gamma stimulation might disrupt it. We further predicted that 20 Hz tACS would alter the braking component of a dependent process computational model. In addition, we investigated the degree of oscillatory entrainment in the EEG following stimulation (i.e., on unstimulated intervals) and assessed whether the behavioral effect of tACS scales according to the strength of the simulated electric field derived from individual neuroanatomy.

RESULTS AND DISCUSSION

All participants (N = 36) tolerated the stimulation well as indicated by the low ratings of discomfort and fatigue, and the ratings did not differ between the two stimulation sessions (Table S1).

General task performance during 20 and 70 Hz stimulation

The independent race model used to estimate SSRT assumes that the distribution of the finishing times of the go process is the same on go and stop trials (context independence). In practice, this means that the average goRT should be higher than the average RT on failed stop trials, i.e., only the fastest go processes are able to escape inhibition. One participant was excluded from all further analyses because of violation of this assumption, resulting in a total of 35 participants (Verbruggen et al., 2019).

The number of errors on go trials was matched between stimulation frequencies ($F_{(1,102)} = 0.14$, $p = 0.71$) and stimulated versus unstimulated trials ($F_{(1,102)} = 0.04$, $p = 0.85$) (Table 1). The dynamic tracking procedure resulted in a stop success rate close to 50% in both stimulation sessions (no main effect of tACS FREQUENCY: $F_{(1,102)} = 0.8$, $p = 0.36$). However, the stop success rate was consistently ~0.5% higher in stimulated than unstimulated trials ($F_{(1,102)} = 26.8$, $p < 0.0001$). Besides a real effect of stimulation, this could also be caused by the difference in trial numbers between the conditions (40% of all trials were stimulated).

20 Hz stimulation reduced force production on stop-signal trials

In corroboration with Joundi et al. (2012), the percent change calculations revealed that 20 Hz stimulation significantly decreased peak force and peak force rate on successful stop trials by 11.02 and 9.8%, respectively (Table 2, Figures 2A and 2C). Due to the reduction in force output, 20 Hz stimulation also shortened the time to peak by 2.77% in successful stop trials. In addition, the proportion of successful stop trials with perfect inhibition, i.e., a force trace that remained below 5 times the SD of the baseline period, increased by 4.23% with 20 Hz stimulation. On go trials, 20 Hz stimulation did not affect peak force rate or the time to peak but did result in a 0.48% increase in mean peak force (Table 2). This might seem counterintuitive and contradicts the findings from Joundi et al. (2012). However, it has been demonstrated before that

Table 2. Force outcomes on Go and successful Stop trials, with 20Hz or 70Hz stimulation ON or OFF

	20Hz				70Hz										
	Go		Successful Stop		Go		Successful Stop		LME statistics						
	OFF	ON	OFF	ON	OFF	ON	OFF	ON	df, Error df	tACS FREQ (20Hz, 70Hz)	STIM (ON,OFF)	TRIAL TYPE (succ stop,go)	tACS FREQ* STIM	tACS FREQ* TYPE	STIM* TYPE	tACS FREQ* STIM* TYPE
Peak force (N)	22.82 ±7.79	22.91 ±7.79	4.38 ±4.16	4.1 ±4.24	23.98 ±7.31	24.09 ±7.34	4.32 ±4.31	4.13 ±4.27	1, 34,353	**F = 239.88 p < 0.0001**	F = 0.02 p = 0.875	**F = 76,547.6 p < 0.0001**	F = 0.08 p = 0.778	**F = 81.52 p < 0.0001**	**F = 6.04 p = 0.014**	F = 0.11 p = 0.740
%change	**0.48 ±1.41 t = 2.04, p = 0.05**		**−11.02 ±22.23 t = -2.93, p = 0.006**		0.42 ± 1.45 t = 1.7, p = 0.1		−6.17 ± 26.55 t = −1.37, p = 0.18									
Peak force rate (N/s)	296.04 ±103.2	297.27 ±103.8	74.57 ±66.96	69.84 ±68.44	304.14 ±95.09	305.68 ±96.14	72.85 ±70.50	70.45 ±69.47	1, 34,289	**F = 42.21 p < 0.0001**	F = 0.11 p = 0.742	**F = 53,017.8 p < 0.0001**	F = 0.43 p = 0.513	**F = 22.91 p < 0.001**	**F = 6.29 p = 0.012**	F = 0.16 p = 0.688
%change	0.21 ± 1.68 t = 0.75, p = 0.46		**−9.8 ±22.23 t = -2.61, p = 0.014**		0.36 ± 1.73 t = 1.23, p = 0.23		−4.13 ± 25.25 t = −0.97, p = 0.34									
Time to peak (ms)	147.75 ±47.57	148.17 ±48.37	99.63 ±50.94	98.07 ±50.46	150.79 ±47.01	151.04 ±47.77	100.46 ±51.95	99.45 ±51.91	1, 33,329	**F = 13.11 p < 0.001**	F = 0.097 p = 0.755	**F = 8094.4 p < 0.001**	F = 0.66 p = 0.417	F = 1.324 p = 0.25	F = 3.031 p = 0.082	F = 0.029 p = 0.864
%change	0.47 ± 2.17 t = 1.27, p = 0.21		**−2.77 ±7.18 t = -2.28, p = 0.03**		0.003 ± 2.8 t = 0.0, p = 0.99		−2.53 ± 12.88 t = −1.16, p = 0.25									
Proportion of trials with force >5* baseline SD			0.81 ±0.12	0.77 ±0.13			0.81 ±0.11	0.78 ±0.15	1, 102			F = 0.062 p = 0.804	**F = 4.707 p = 0.032**		F = 0.161 p = 0.689	
%change			**−4.23 ±9.66 t = -2.59, p = 0.014**				−3.25 ± 10.92 t = −1.76, p = 0.09									

Mean ± SD is reported. LME = linear mixed model. Results for LME models are given as Type III sums of squares for sequentially fitted fixed effects. Statistically significant findings are highlighted in bold.

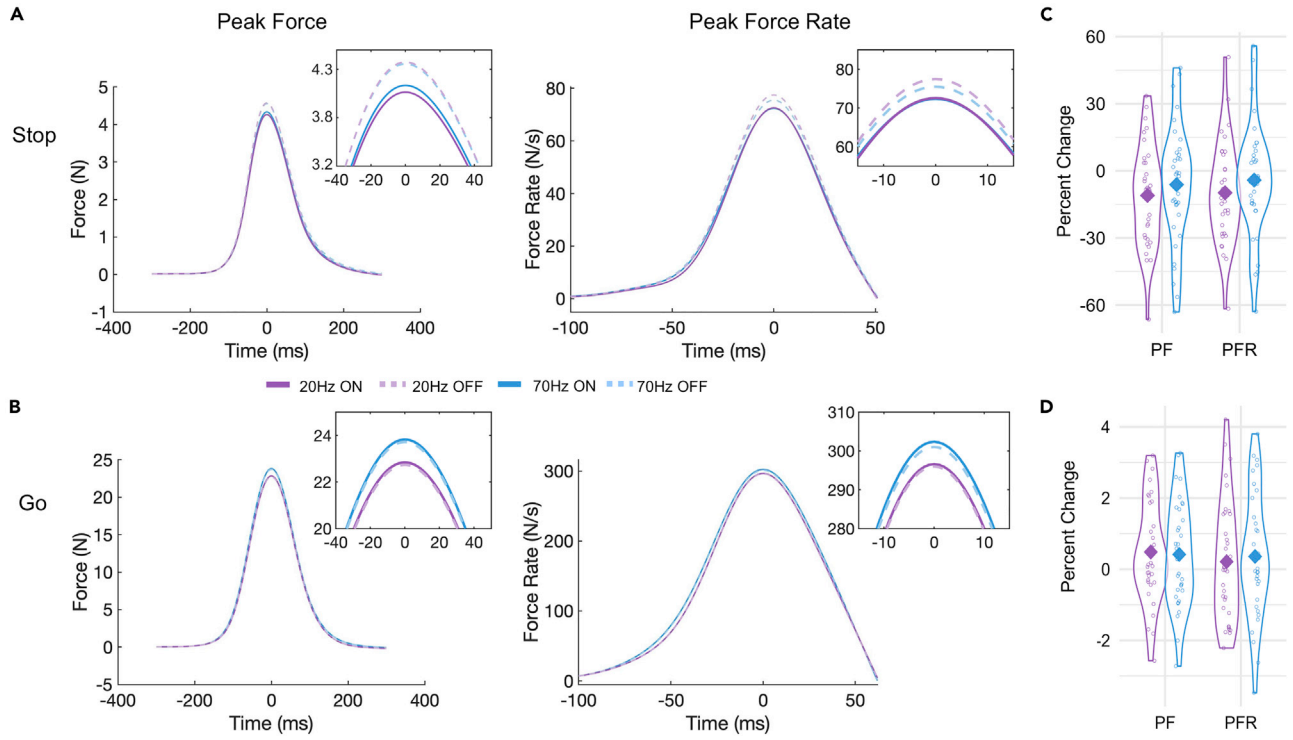

Figure 2. Force results

(A and B) Grand averages for stop (A) and go (B) aligned to peak force and peak force rate for 20 Hz (purple) and 70 Hz (blue) stimulated (solid lines) and unstimulated (dashed lines) trials. Sub-windows depict a zoomed-in view on the peaks.

(C and D) Individual percent changes of peak force and peak force rate because of 20 Hz (purple) and 70 Hz (blue) stimulation on stop (C) and go (D) trials. Solid diamond shape represents the group mean. PF = peak force, PFR = peak force rate.

the response force on go trials increases with the increasing likelihood of a stop-signal appearing, in other words, when the readiness to respond is low (Van Den Wildenberg et al., 2003). Analogous to the relationship between excessive beta oscillation and the bradykinesia and rigidity symptoms in PD (Kuhn et al., 2006), we speculate that 20Hz stimulation puts a global break on the system, making it harder to respond when necessary. There in also lies an important difference between the go/no-go task used by Joundi and colleagues and our anticipated response stop-signal paradigm. In the go/no-go task, there is no hard constraint on when to respond other than the experimenter's instruction to respond as fast as possible. As a result, participants tend to slow down until they gather enough evidence for going (Leunissen et al., 2017; Szmalec et al., 2009). Here, participants needed to perform a response at a known point in time, and on top of that there was visual feedback on their performance, reinforcing go task performance.

Higher force production on go trials in the 70 Hz stimulation session

Peak force and peak force rate were significantly higher in the 70 Hz than in the 20 Hz stimulation session (Table 2, Figure 2B). This effect seemed to be driven by the go trials (significant TRIAL TYPE* tACS FREQUENCY interaction; estimated difference in peak force on go trials: 1.09 $\pm$ 0.06N, z = 17.44, $p_{adjusted}$ < 0.0001, stop trials: −0.15 $\pm$ 0.12N, z = −1.24, $p_{adjusted}$ = 0.592; estimated difference in mean peak force rate on go trials: 6.84 $\pm$ 0.9N/s, z = 7.61, $p_{adjusted}$ <0 .0001, stop trials: −2.62 $\pm$ 1.76N/s, z = −1.49, $p_{adjusted}$ = 0.433). The percent change calculations show that peak force on stimulated go trials in the 70 Hz stimulation session was 0.42% higher than peak force on the unstimulated go trials. This increase was not significant however (p = 0.1). Because there was no effect of stimulation ON/OFF or a separate sham session, it is impossible to infer whether the difference in force on go trials between the 20 and 70 Hz session is caused by a decrease because of 20 Hz stimulation or an increase because of 70 Hz stimulation. Based on the findings from Joundi et al. (2012), the most likely scenario is perhaps a combination of both.

The lack of differences between stimulated and unstimulated go trials in the 70 Hz stimulation session could be caused by several factors. First, the preSMA and SMA-proper are thought to be responsible for linking situations with appropriate actions (Nachev et al., 2008). Hosaka et al. (2016) demonstrated that gamma oscillatory activity in the (pre)SMA of monkeys increased during movement but particularly when the action plan needed to be updated. Second, given the significant difference in peak force and peak force rate between the 20 and 70 Hz stimulation session, it is also possible that the stimulation effects carried over to the unstimulated trials (see tACS aftereffects section for a more in-depth discussion).

Opposing effects of 20 and 70 Hz stimulation on braking drift rate

Similarly to Pogosyan et al. (2009) and Joundi et al. (2012), no difference in goRT was observed between the different stimulation frequencies or stimulation ON/OFF (Table 1).

SSRT was significantly shorter in the 20 Hz than in the 70 Hz stimulation session ($F_{(1,102)} = 5.36$, $p = 0.023$), but there was no difference between SSRT estimated from stimulated and unstimulated trials or a FREQUENCY*STIMULATION interaction. Again, this precludes us from concluding whether 70 Hz stimulation increased SSRT or 20 Hz stimulation decreased SSRT.

SSRT is an estimate of the covert latency of the stop signal estimated based on the independent race model (Logan et al., 1984). Conceptualizing the go and stop processes as independent processes racing against each other has accounted well for the observed behavioral data in the stop-signal paradigm (Matzke et al., 2018). However, on a neural level, it is evident that the neurons involved in movement initiation and inhibition interact with each other during action cancellation (Boucher et al., 2007; Munoz and Schall, 2003; Schmidt et al., 2013). Models that include such a dependency between the go and stop process indeed provide an even better fit to the behavioral data (Boucher et al., 2007; Dunovan et al., 2015). In the dependent process model (DPM), (Dunovan et al., 2015, Dunovan and Verstynen, 2019) the go process is modeled as a stochastic accumulator that gathers evidence at a certain drift-rate (v_e), leading to a response when it crosses an upper threshold (a) (Figure 3). In the event of a stop-signal, a second braking process is instantiated at the current state of the execution process and must reach the bottom boundary before the execution threshold is reached to cancel motor output. This model not only provides a better fit to the data but also gives insight into the mechanisms underlying going and stopping. Another advantage is that the DPM takes the full goRT and failed stop RT distributions into account. Even though there was no difference in average goRT and SSRT between stimulated and unstimulated trials, stimulation might have altered the shape of the response distributions. By fitting the DPM, differences in shape can be picked up and are reflected in a change in the rate of the execution (v_e) or braking drift (v_b), shift the onset time at which the execution process begins to accumulate (tr), or change the distance to the threshold (a).

The DPM was fitted to the group data, and although all models provided a good fit to the data, the braking drift modulation model best explained the effect of stimulation on task performance (Figure 4, Table 3). Braking drift rate increased because of 20 Hz stimulation, whereas 70 Hz stimulation decreased the braking drift rate (note that more negative values reflect a stronger braking process).

Taken together, the results from the force and response time analyses show opposing roles for beta and gamma oscillations that fit with the prevailing view that gamma activity in the motor system is prokinetic, whereas beta oscillations support motor suppression.

The role of gamma oscillatory activity during motor inhibition

Considering that gamma oscillations in the motor system are regarded as prokinetic, one would expect them to decrease during successful inhibition. Although there is some evidence for decreased gamma-band power (Alegre et al., 2013), most intracranial electrophysiology studies have reported a brief *increase* centered around 70 Hz in response to a stop-signal. This phenomenon has been observed in the preSMA, rIFC (Bartoli et al., 2018; Fonken et al., 2016; Swann et al., 2012), and the STN (Fischer et al., 2017; Ray et al., 2012). Generally, this increased gamma activity was present regardless of the success of stopping but before SSRT (but see Fischer et al., 2017). It is unclear if it reflects an attentional signature for detecting the stop-signal or if it might be involved in the actual implementation of the inhibitory process.

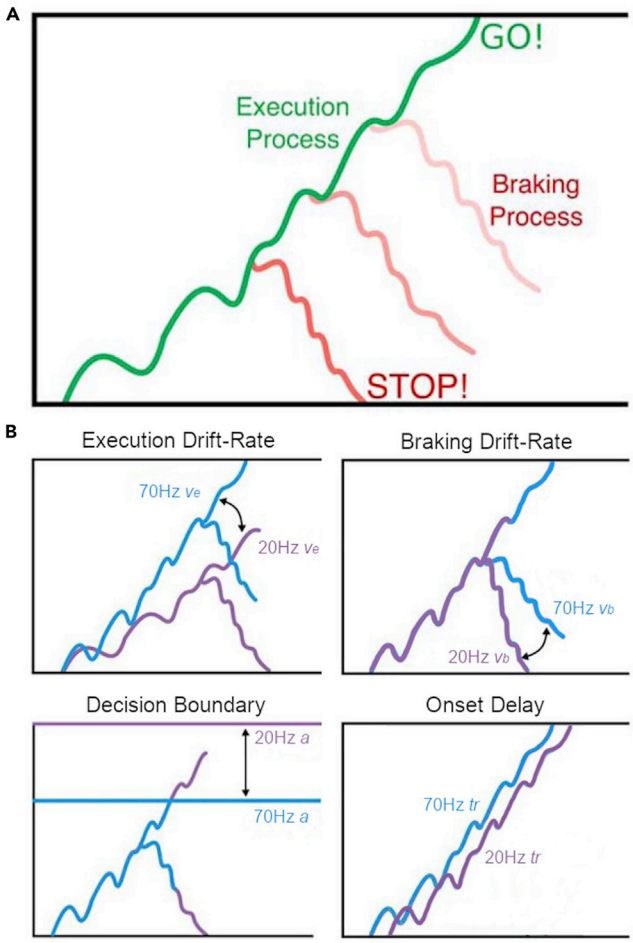

Figure 3. Graphical description of the dependent process model (DPM)

(A) The DPM assumes that the state of an accumulating execution process at the time of the stop-signal determines the initial state of the braking process, making it more difficult to cancel actions closer to the execution boundary.

(B) Possible control mechanisms that could be altered by beta (20 Hz) and/or gamma (70 Hz) tACS stimulation. Adapted with permission from Dunovan and Verstynen (2019).

Here, we did not find evidence for a causal role of gamma oscillations in stopping. Gamma stimulation even seemed to reduce the speed of the braking process and rather affected go performance. Peak force and peak force rate were higher in the 70 Hz stimulation session. Moreover, the parameter estimates of the DPM's all point toward movement facilitation with 70 Hz stimulation (i.e., increased execution drift rate, lower boundary heights, and shorter onset delay). Fischer et al. (2017) suggested that comparisons between executed and withheld movements might reflect the lack of movement rather than the stopping process per se. By using a task in which continuous ongoing movement needs to be inhibited, they circumvent this issue,and based on their findings, they advocate that increased gamma and not beta activity is responsible for successful inhibition. We want to emphasize that our paradigm was very successful in ensuring go response initiation, since the proportion of successful stop trials in which we could still identify a force response five SD above baseline was on average 80% (range 50–100%, Table 2) opposed to ~45% in Joundi et al. (2012). Therefore, we find this explanation unlikely for our findings.

Gamma activity is thought to reflect local activity, whereas beta band activity seems important for long-distance communication between frontal cortex and the basal ganglia (Bartoli et al., 2018; Swann et al., 2012). This long-distance communication might require less precise timing of the entrainment. Because preSMA gamma-band activity increases for both going and stopping (albeit at different timescales) trials, stimulating at 70 Hz for the whole trial duration might create a conflict between facilitating movement versus promoting inhibition.

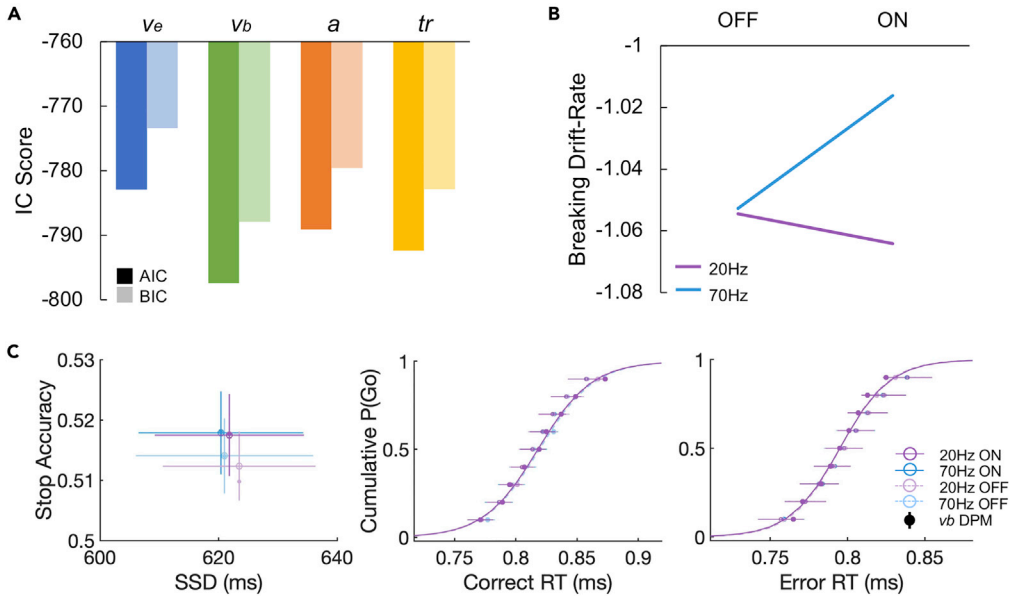

Figure 4. Dependent process model (DPM) results

(A) Goodness-of-fit measures for the four different dependent process models. AIC (dark) and BIC (light) scores for all single-parameter models, allowing either execution drift-rate (v_e; blue), braking drift-rate (v_b; green), execution boundary height (*a*; orange), or onset delay (*tr*; yellow) to vary across conditions. The model with the lowest score, in this case the braking drift modulation model, is preferred.

(B) Parameter estimates of the braking drift rate in stimulated and unstimulated trials in the beta (20 Hz) and gamma (70 Hz) sessions.

(C) Model predicted data (solid lines and circles) simulated with best-fit parameters from the v_b model overlaid on the average ± SEM empirical data (transparent circles and horizontal lines).

Sources of variability

The behavioral results largely follow the hypothesized effects of stimulation. However, it is also evident that the effects are variable from one participant to the next and are state-dependent, e.g., 20 Hz tACS had a much stronger effect on stop-signal trials than go trials. In an attempt to identify some possible sources of this variability, we performed several exploratory analyses.

Electrical field modeling

The amount of current that reaches the targeted brain area likely influences the stimulation effect. Stimulation was provided at a fixed output current of 1mA, but individual differences (e.g., in skull thickness and scalp to cortex distance) can influence how much current actually reaches the brain (Datta et al., 2012). To investigate whether there was a dose-response relationship between amount of current reaching the pre-SMA and the behavioral effect of stimulation, we modeled the current flow in each individual (N = 18) based on the registered electrode positions and MRI scans. Two recent studies provide validation for the accuracy of such models by using intracranial recordings (Huang et al., 2017; Opitz et al., 2016).

The modeling results indicated that, on average, the current successfully reached the preSMA and that the field expansion was limited to the area between the four return electrodes (Figure 5A). The predicted normalized electric field strength in the preSMA ROI during the beta session was significantly related to the percent change in peak force on successful stops ($r = -0.469$, $p = 0.028$) (Figure 5B). This dose-response relationship supports the notion that tACS stimulation has a causal effect on behavior and suggests that it would be advisable to try to control the amount of current to the brain by adjusting the output current based on the current flow predictions (Bestmann and Ward, 2017; Tan et al., 2020).

Aftereffect of beta stimulation is state-dependent

The central tACS electrode was placed under channel FCz; therefore, we focused our analyses on channel Fz, which lies directly in front of FCz and still covers the preSMA. To give further justification for this choice,

Table 3. Dependent process model parameter estimates and fit statistics

	Flat model	20Hz Unstimulated	20Hz Stimulated	70Hz Unstimulated	70Hz Stimulated	AIC	BIC	Δ with v_b model
v_e	1.198	1.197	1.197	1.997	1.999	−782.939	−773.411	14.485
v_b	−1.052	−1.054	−1.064	−1.053	−1.016	−797.424	−787.896	
a	0.443	0.439	0.443	0.442	0.434	−789.094	−779.656	8.24
tr	0.44996	0.44996	0.44996	0.44999	0.44969	−792.392	−782.864	5.032

Best fit parameter estimates for braking drift rate (v_b), execution drift rate (v_e), boundary height (*a*) and onset delay (*tr*). The last two columns show the Akaike information criterion (AIC), and Bayesian information criterion (BIC) as complexity penalized goodness-of-fit measures. Lower values in all three measures imply a better fit to the data.

we contrasted all unstimulated successful stop (∼60) and go (∼244) trials from both sessions with each other. This comparison revealed one significant positive cluster ($p = 0.0002$) with a fronto-central topography in which the beta activity was higher for successful stop trials than in go trials from 150 until 400ms after the presentation of the stop signal. This cluster includes electrode Fz and extends to electrodes covering the rIFC (Figures 6A and 6B). Moreover, participants with higher Fz beta activity 150 ms after the stop signal had shorter SSRTs (average unstimulated SSRT over both sessions, $r = -0.44$, $p_{adjustedr} = 0.034$) (Figure 6C).

Ideally one would be able to assess changes in oscillatory activity *during* tACS. However, it remains unresolved whether the tACS artifact can be proficiently removed from concurrent magnetoencephalography and electroencephalography (M/EEG) recordings (Neuling et al., 2017; Noury and Siegel, 2018). The lack of behavioral differences between trials with and without stimulation might be because of the stimulation effects outlasting the stimulation train. Our intermittent tACS design allows for the comparison between EEG spectral power in trials directly following stimulation with those further removed from the stimulation (also see Figure S2 for comparison of spectral power in pre-/post tACS resting EEG measurements). Comparing successful stop trials directly following stimulation (i.e., stop-signal was presented ∼2.5 s after the end of the previous stimulation train, ∼38 trials) with successful stop trials following a unstimulated trial (i.e., stop-signal was presented ∼7 s after the of end of the previous stimulation train, ∼21 trials) revealed one significant positive cluster with higher beta activity, ranging between 13 and 19 Hz, 250-50 ms before the presentation of the stop signal in trials directly following 20 Hz stimulation (Figure 6D). This effect was not present in the 70 Hz stimulation session or in go trials (Figure 6E). Under normal circumstances, beta activity starts to desynchronize ∼300ms before the target line in preparation of the response. On stop trials beta activity quickly resynchronizes again after the stop signal (Figure 6A) (Swann et al., 2012; Wagner et al., 2018; Wessel et al., 2016). The finding that beta activity in preSMA was increased 200ms *before* the stop-signal (i.e., before participants knew for certain they had to stop) suggests that when participants proactively activated the inhibition network in anticipation of a stop signal in trials following a stimulation train, the endogenous beta oscillations were still enhanced. This highlights that the (after-)effects of tACS are state-dependent, i.e., entrainment particularly takes place when endogenous oscillations with a frequency close to the stimulation frequency are naturally present.

Individual peak frequency

Another possible source of variability is the stimulation frequency. The effects of tACS seem to follow an Arnold tongue principle in the sense that tACS can only modulate ongoing brain oscillations if the frequency of the tACS is very close to the frequency of the intrinsic brain oscillations. To be able to synchronize or entrain frequencies further away from the "Eigenfrequency" the external driving force (tACS) will need to be stronger (i.e., higher stimulation amplitude) (Ali et al., 2013). In this study, we chose to use 20 and 70 Hz as stimulation frequencies because oscillatory activity in the motor system is commonly centered around these frequencies (Chakarov et al., 2009; Fischer et al., 2017; Muthukumaraswamy, 2010). To evaluate whether individuals with a peak in beta oscillatory power close to 20 Hz responded more strongly to the stimulation than individuals with a peak frequency further removed from 20 Hz, we identified the individual beta frequency based on the resting state EEG acquired before the beta stimulation session and plotted it against the percent change in force on successful stop trials.

Figure S3 demonstrates that participants with a peak between 18 and 22 Hz typically showed a decrease in peak force on successful stops with beta stimulation for 23/27 participants (85%), whereas

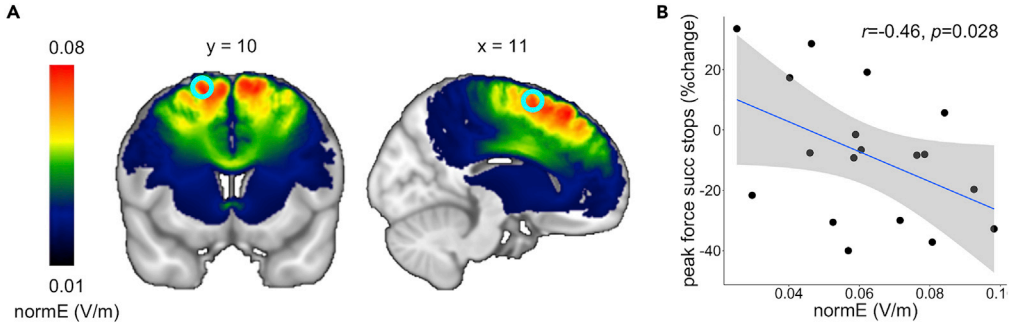

Figure 5. Simulation of the electrical field of the tACS

(A) Group average (N = 18) of the normalized predicted electrical field distribution of the white and gray matter in MNI space. Note that the efield predictions for the CSF were not transformed to MNI space explaining the interhemispheric gap in the efield model. The cyan circle indicates the preSMA ROI (10 mm sphere around coordinate [11,10,62] based on a previous fMRI study with the same task paradigm).

(B) Relation between normalized predicted electrical field strength within the preSMA ROI and the effect of beta stimulation on peak force in successful stop trials. The shaded area represents the 95% confidence interval.

outside of that range 3/8 participants (37%) showed a decrease. This corroborates with findings from Vossen et al. (2015) who found the aftereffects of alpha stimulation to be the strongest at the individual alpha peak and not present ±2 Hz away from the individual peak frequency. Note that a similar procedure is not possible for the gamma-band, as the signal to noise ratio with scalp EEG makes it difficult to reliably uncover the higher frequencies and gamma-band activity is typically quite broad without a clear individual peak.

Limitations of the study

The difference in beta power between unstimulated stop trials directly following stimulation and those following a unstimulated trial illustrate that the effects of our intermittent stimulation protocol carried over to the unstimulated trials and likely clouded the differences between stimulation ON/OFF, similar to the offline effects reported in Heise et al. (2019). It would be recommendable to include a sham session even when using an intermittent stimulation protocol.

In addition, it should be noted that the current densities within the preSMA ROI are lower than the electric field strengths typically reported (>0.1–0.5 V/m) to be sufficient to affect spike timing and cause direct neural entrainment (Deans et al., 2007; Voroslakos et al., 2018; Johnson et al., 2020; Reato et al., 2010; Chan and Nicholson, 1986; Krause et al., 2019; Tran et al., 2022). Maximal current densities achieved in the brain tissue ranged between 0.05 and 0.28 V/m (average: 0.13 V/m) in this study. The effects of electric fields on spike entrainment have been shown to be continuous and linearly related to the electric field strength (Deans et al., 2007; Voroslakos et al., 2018; Johnson et al., 2020). Thus, very low electrical fields could still result in neural entrainment, albeit only in a small proportion of neurons. It is unclear how tACS effects might be magnified by dynamic network activity when engaged in a task. Therefore, we cannot exclude the possibility that (part) of our findings are caused by indirect neural entrainment, for example via transcutaneous mechanisms (Asamoah et al., 2019). These limitations need further investigation, which is crucial for understanding the reliability of tACS application.

Conclusion

We provide evidence that fronto-central beta oscillatory activity is causal to stopping ability. During successful stop trials, 20 Hz stimulation over preSMA resulted in a considerable decrease in force output, and the response time models revealed that 20 Hz stimulation specifically increased braking drift. These effects followed a dose-response relationship with the strength of the individually simulated electric field. In contrast, 70 Hz stimulation decreased braking drift but primarily affected go task performance. Our results highlight the state-dependency of tACS entrainment and along with recent complementary research (Sundby et al., 2020) pave the way for the use of fronto-central beta activity as a functional marker of motor inhibition.

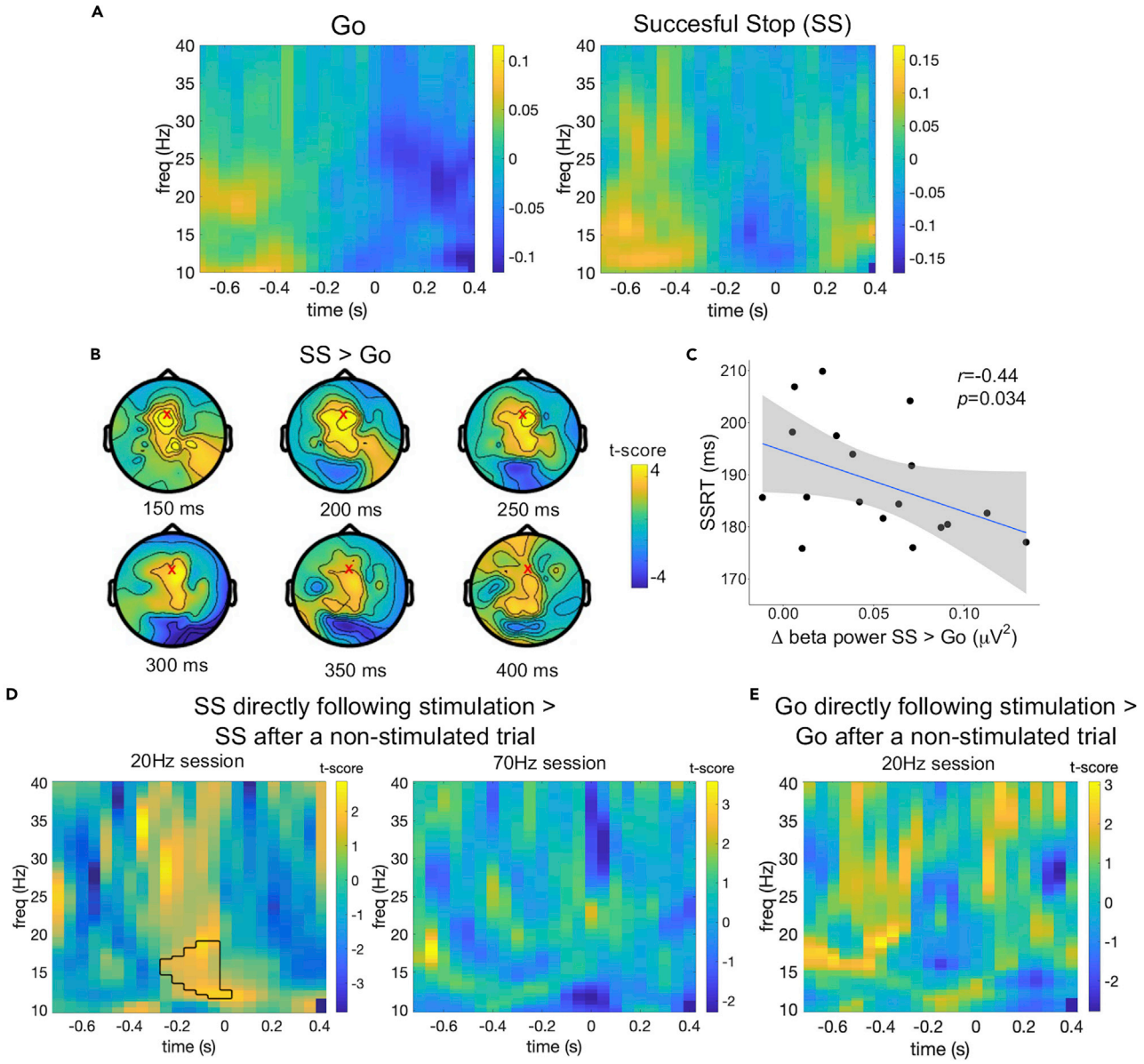

Figure 6. EEG results

(A) Go and Successful stop trial time-frequency results (N = 18), time locked to the (average) stop signal presentation (t = 0). Colormap represents the normalized change with respect to the baseline from −0.4-0s before the stop signal.

(B) Topographic distribution of increased beta activity in successful stops versus go trials 150-400ms after the presentation of the stop signal. The red X marks the location of electrode Fz.

(C) Correlation between the difference in beta power for successful stop and go trials 150ms after the presentation of the stop signal and stop-signal reaction time (SSRT) in electrode Fz. The shaded area represents the 95% confidence interval.

(D) Time-frequency power plots of the comparison between successful stop trials that directly followed stimulation and successful stop trials that occurred after a unstimulated trial. The black outline represents the significant positive cluster.

(E) Time-frequency power plots of the comparison between go trials that directly followed stimulation and go trials that occurred after a unstimulated trial.

STAR★METHODS

Detailed methods are provided in the online version of this paper and include the following:

- KEY RESOURCES TABLE
- RESOURCE AVAILABILITY

SUPPLEMENTAL INFORMATION

Supplemental information can be found online at https://doi.org/10.1016/j.isci.2022.104338.

ACKNOWLEDGMENTS

This work was supported by the Internal Research Fund KU Leuven (C16/15/070), Research Foundation Flanders (FWO) grants (G089818N, G0F7616N, G093616N, and I005018N) and an Excellence of Science grant (EOS 30446199, MEMODYN), awarded to S.P.S.., D.M., and coworkers. I.L. is supported by an individual fellowship of the FWO (12M6718N) and EU (Marie Skłodowska-Curie Actions [MSCA] 798619). J.C. is supported by the Australian Research Council (ARC DP200100234 and DP180102066) and the Office of Naval Research Global (N62909-18-1-2174).

AUTHOR CONTRIBUTIONS

Conceptualization, I.L., J.P.C., and S.P.S.; Methodology, I.L., K.F.H., T.S.M., D.M., and J.P.C.; Software, K.D.; Investigation, M.V.S. and I.L.; Formal Analysis, M.V.S. and I.L.; Writing – Original Draft, M.V.S. and I.L.; Writing – Review & Editing, K.F.H., T.S.M., K.D., D.M., J.P.C, and S.P.S.; Funding Acquisition, I.L., J.P.C., and S.P.S.; Resources, S.P.S.; Supervision, J.P.C. and S.P.S.

DECLARATION OF INTERESTS

The authors declare no competing interests.

Received: September 24, 2021
Revised: January 14, 2022
Accepted: April 27, 2022
Published: May 20, 2022

REFERENCES

Alegre, M., Lopez-Azcarate, J., Obeso, I., Wilkinson, L., Rodriguez-Oroz, M.C., Valencia, M., Garcia-Garcia, D., Guridi, J., Artieda, J., Jahanshahi, M., and Obeso, J.A. (2013). The subthalamic nucleus is involved in successful inhibition in the stop-signal task: a local field potential study in Parkinson's disease. Exp. Neurol. *239*, 1–12.

Ali, M.M., Sellers, K.K., and Frohlich, F. (2013). Transcranial alternating current stimulation modulates large-scale cortical network activity by network resonance. J. Neurosci. *33*, 11262–11275.

Aron, A.R., Herz, D.M., Brown, P., Forstmann, B.U., and Zaghloul, K. (2016). Frontosubthalamic circuits for control of action and cognition. J. Neurosci. *36*, 11489–11495.

Asamoah, B., Khatoun, A., and Mc Laughlin, M. (2019). Tacs motor system effects can Be caused by transcutaneous stimulation of peripheral nerves. Nat. Commun. *10*, 266.

Bartoli, E., Aron, A.R., and Tandon, N. (2018). Topography and timing of activity in right inferior frontal cortex and anterior insula for stopping movement. Hum. Brain Mapp. *39*, 189–203.

Bestmann, S., and Ward, N. (2017). Are current flow models for transcranial electrical stimulation fit for purpose? Brain Stimul. *10*, 865–866.

Bikson, M., Datta, A., and Elwassif, M. (2009). Establishing safety limits for transcranial direct current stimulation. Clin. Neurophysiol. *120*, 1033–1034.

Bissett, P.G., and Logan, G.D. (2012). Post-stop-signal slowing: strategies dominate reflexes and implicit learning. J. Exp. Psychol. Hum. Percept. Perform. *38*, 746–757.

Boucher, L., Palmeri, T.J., Logan, G.D., and Schall, J.D. (2007). Inhibitory control in mind and brain: an interactive race model of countermanding saccades. Psychol. Rev. *114*, 376–397.

Castiglione, A., Wagner, J., Anderson, M., and Aron, A.R. (2019). Preventing A thought from coming to mind elicits increased right frontal beta just as stopping action does. Cereb. Cortex *29*, 2160–2172.

Chakarov, V., Naranjo, J.R., Schulte-Monting, J., Omlor, W., Huethe, F., and Kristeva, R. (2009). Beta-range eeg-emg coherence with isometric compensation for increasing modulated low-level forces. J. Neurophysiol. *102*, 1115–1120.

Chan, C.Y., and Nicholson, C. (1986). Modulation by applied electric fields of purkinje and stellate cell activity in the isolated turtle cerebellum. J. Physiol. *371*, 89–114.

Coxon, J.P., Stinear, C.M., and Byblow, W.D. (2006). Intracortical inhibition during volitional inhibition of prepared action. J. Neurophysiol. *95*, 3371–3383.

Coxon, J.P., Goble, D.J., Leunissen, I., Van Impe, A., Wenderoth, N., and Swinnen, S.P. (2016). Functional brain activation associated with inhibitory control deficits in older adults. Cereb. Cortex *26*, 12–22.

Crone, N.E., Miglioretti, D.L., Gordon, B., and Lesser, R.P. (1998). Functional mapping of human sensorimotor cortex with electrocorticographic spectral analysis. II. Event-related synchronization in the gamma band. Brain *121*, 2301–2315.

Datta, A., Truong, D., Minhas, P., Parra, L.C., and Bikson, M. (2012). Inter-individual variation during transcranial direct current stimulation and normalization of dose using mri-derived computational models. Front. Psychiatry *3*, 91.

Deans, J.K., Powell, A.D., and Jefferys, J.G. (2007). Sensitivity of coherent oscillations in rat Hippocampus to Ac electric fields. J. Physiol. *583*, 555–565.

Dunovan, K., Lynch, B., Molesworth, T., and Verstynen, T. (2015). Competing basal ganglia pathways determine the difference between stopping and deciding not to go. Elife *4*, E08723.

Dunovan, K., and Verstynen, T. (2019). Errors in action timing and inhibition facilitate learning by tuning distinct mechanisms in the underlying decision process. J. Neurosci. *39*, 2251–2264.

Engel, A.K., and Fries, P. (2010). Beta-band oscillations–signalling the status quo? Curr. Opin. Neurobiol. *20*, 156–165.

Fischer, P., Pogosyan, A., Herz, D.M., Cheeran, B., Green, A.L., Fitzgerald, J., Aziz, T.Z., Hyam, J., Little, S., Foltynie, T., et al. (2017). Subthalamic nucleus gamma activity increases not only during movement but also during movement inhibition. Elife *6*, e23947.

Fonken, Y.M., Rieger, J.W., Tzvi, E., Crone, N.E., Chang, E., Parvizi, J., Knight, R.T., and Kramer, U.M. (2016). Frontal and motor cortex contributions to response inhibition: evidence from electrocorticography. J. Neurophysiol. *115*, 2224–2236.

Fries, P. (2005). A mechanism for cognitive dynamics: neuronal communication through neuronal coherence. Trends Cogn. Sci. *9*, 474–480.

Guerra, A., Bologna, M., Paparella, G., Suppa, A., Colella, D., Di Lazzaro, V., Brown, P., and Berardelli, A. (2018). Effects of transcranial alternating current stimulation on repetitive finger movements in healthy humans. Neural Plast. *2018*, 4593095.

Haegens, S., Cousijn, H., Wallis, G., Harrison, P.J., and Nobre, A.C. (2014). Inter- and intra-individual variability in alpha peak frequency. Neuroimage *92*, 46–55.

Heise, K.F., Monteiro, T.S., Leunissen, I., Mantini, D., and Swinnen, S.P. (2019). Distinct online and offline effects of alpha and beta transcranial alternating current stimulation (tacs) on continuous bimanual performance and task-set switching. Sci. Rep. *9*, 3144.

Helfrich, R.F., Schneider, T.R., Rach, S., Trautmann-Lengsfeld, S.A., Engel, A.K., and Herrmann, C.S. (2014). Entrainment of brain oscillations by transcranial alternating current stimulation. Curr. Biol. *24*, 333–339.

Herrmann, C.S., Struber, D., Helfrich, R.F., and Engel, A.K. (2016). Eeg oscillations: from correlation to causality. Int. J. Psychophysiol. *103*, 12–21.

Homan, R.W., Herman, J., and Purdy, P. (1987). Cerebral location of international 10-20 system electrode placement. Electroencephalogr. Clin. Neurophysiol. *66*, 376–382.

Hosaka, R., Nakajima, T., Aihara, K., Yamaguchi, Y., and Mushiake, H. (2016). The suppression of beta oscillations in the primate supplementary motor complex reflects A volatile state during the updating of action sequences. Cereb. Cortex *26*, 3442–3452.

Hothorn, T., Bretz, F., and Westfall, P. (2008). Simultaneous inference in general parametric models. Biom. J. *50*, 346–363.

Huang, Y., Liu, A.A., Lafon, B., Friedman, D., Dayan, M., Wang, X., Bikson, M., Doyle, W.K., Devinsky, O., and Parra, L.C. (2017). Measurements and models of electric fields in the in vivo human brain during transcranial electric stimulation. Elife *6*, e18834.

Huskisson, E.C. (1974). Measurement of pain. Lancet *2*, 1127–1131.

Huster, R.J., Schneider, S., Lavallee, C.F., Enriquez-Geppert, S., and Herrmann, C.S. (2017). Filling the void-enriching the feature space of successful stopping. Hum. Brain Mapp. *38*, 1333–1346.

Jahanshahi, M., Obeso, I., Rothwell, J.C., and Obeso, J.A. (2015). A fronto-striato-subthalamic-pallidal network for goal-directed and habitual inhibition. Nat. Rev. Neurosci. *16*, 719–732.

Jha, A., Nachev, P., Barnes, G., Husain, M., Brown, P., and Litvak, V. (2015). The frontal control of stopping. Cereb. Cortex *25*, 4392–4406.

Johnson, L., Alekseichuk, I., Krieg, J., Doyle, A., Yu, Y., Vitek, J., Johnson, M., and Opitz, A. (2020). Dose-dependent effects of transcranial alternating current stimulation on spike timing in awake nonhuman primates. Sci. Adv. *6*. https://doi.org/10.1126/sciadv.aaz2747.

Joundi, R.A., Jenkinson, N., Brittain, J.S., Aziz, T.Z., and Brown, P. (2012). Driving oscillatory activity in the human cortex enhances motor performance. Curr. Biol. *22*, 403–407.

Krause, M.R., Vieira, P.G., Csorba, B.A., Pilly, P.K., and Pack, C.C. (2019). Transcranial alternating current stimulation entrains single-neuron activity in the primate brain. Proc. Natl. Acad. Sci. U S A *116*, 5747–5755.

Kuhn, A.A., Kupsch, A., Schneider, G.H., and Brown, P. (2006). Reduction in subthalamic 8-35 Hz oscillatory activity correlates with clinical improvement in Parkinson's disease. Eur. J. Neurosci. *23*, 1956–1960.

Kuhn, A.A., Williams, D., Kupsch, A., Limousin, P., Hariz, M., Schneider, G.H., Yarrow, K., and Brown, P. (2004). Event-related beta desynchronization in human subthalamic nucleus correlates with motor performance. Brain *127*, 735–746.

Lee, M.D., and Wagenmakers, E.J. (2014). Bayesian Cognitive Modeling: A Practical Course (Cambridge University Press).

Leunissen, I., Coxon, J.P., and Swinnen, S.P. (2016). A proactive task set influences how response inhibition is implemented in the basal ganglia. Hum. Brain Mapp. *37*, 4706–4717.

Leunissen, I., Zandbelt, B.B., Potocanac, Z., Swinnen, S.P., and Coxon, J.P. (2017). Reliable estimation of inhibitory efficiency: to anticipate, choose or simply react? Eur. J. Neurosci. *45*, 1512–1523.

Little, S., and Brown, P. (2014). The functional role of beta oscillations in Parkinson's disease. Parkinsonism Relat. Disord. *20*, S44–S48.

Litvak, V., Eusebio, A., Jha, A., Oostenveld, R., Barnes, G., Foltynie, T., Limousin, P., Zrinzo, L., Hariz, M.I., Friston, K., and Brown, P. (2012). Movement-related changes in local and long-range synchronization in Parkinson's disease revealed by simultaneous magnetoencephalography and intracranial recordings. J. Neurosci. *32*, 10541–10553.

Logan, G.D., Cowan, W.B., and Davis, K.A. (1984). On the ability to inhibit simple and choice reaction time responses A model and A method. J. Exp. Psychol. Hum. Percept. Perform. *10*, 276–291.

Maris, E., and Oostenveld, R. (2007). Nonparametric statistical testing of eeg- and meg-data. J. Neurosci. Methods *164*, 177–190.

Matzke, D., Verbruggen, F., and Logan, G.D. (2018). The stop-signal paradigm. In Stevens' Handbook of Experimental Psychology and Cognitive Neuroscience (John Wiley & Sons, Inc).

Moisa, M., Polania, R., Grueschow, M., and Ruff, C.C. (2016). Brain network mechanisms underlying motor enhancement by transcranial entrainment of gamma oscillations. J. Neurosci. *36*, 12053–12065.

Munoz, D.P., and Schall, J.D. (2003). Concurrent, distributed control of saccade initiation in the frontal eye field and superior colliculus. In The Superior Colliculus: New Approaches For Studying Sensorimotor Integration, W.T. Hall and A. Moschovakis, eds. (CRC Press).

Muthukumaraswamy, S.D. (2010). Functional properties of human primary motor cortex gamma oscillations. J. Neurophysiol. *104*, 2873–2885.

Muthukumaraswamy, S.D. (2013). High-frequency brain activity and muscle artifacts in meg/eeg: a Review and recommendations. Front. Hum. Neurosci. *7*, 138.

Nachev, P., Kennard, C., and Husain, M. (2008). Functional role of the supplementary and pre-supplementary motor areas. Nat. Rev. Neurosci. *9*, 856–869.

Neuling, T., Ruhnau, P., Weisz, N., Herrmann, C.S., and Demarchi, G. (2017). Faith and oscillations recovered: on analyzing eeg/meg signals during tacs. Neuroimage *147*, 960–963.

Nikulin, V.V., and Brismar, T. (2006). Phase synchronization between alpha and beta oscillations in the human electroencephalogram. Neuroscience *137*, 647–657.

Noury, N., and Siegel, M. (2018). Analyzing eeg and meg signals recorded during tes, A reply. Neuroimage *167*, 53–61.

Oldfield, R.C. (1971). The assessment and analysis of handedness: the edinburgh inventory. Neuropsychologia *9*, 97–113.

Oostenveld, R., Fries, P., Maris, E., and Schoffelen, J.M. (2011). Fieldtrip: open source software for advanced analysis of meg, eeg, and invasive electrophysiological data. Comput. Intell. Neurosci. *2011*, 156869.

Opitz, A., Falchier, A., Yan, C.G., Yeagle, E.M., Linn, G.S., Megevand, P., Thielscher, A., Deborah, A.R., Milham, M.P., Mehta, A.D., and Schroeder, C.E. (2016). Spatiotemporal structure of intracranial electric fields induced by transcranial electric stimulation in humans and nonhuman primates. Sci. Rep. *6*, 31236.

Opitz, A., Paulus, W., Will, S., Antunes, A., and Thielscher, A. (2015). Determinants of the electric field during transcranial direct current stimulation. Neuroimage *109*, 140–150.

Pinheiro, J., Bates, D., Debroy, S., and Sarkar, D.; R Core Team (2021). Linear and Nonlinear Mixed Effects Models (R Core Team). https://CRAN.R-project.org/package=nlme.

Pogosyan, A., Gaynor, L.D., Eusebio, A., and Brown, P. (2009). Boosting cortical activity at beta-band frequencies slows movement in humans. Curr. Biol. *19*, 1637–1641.

R Core Team (2020). R: A Language and Environment for Statistical Computing (R Foundation For Statistical Computing). Https://Www.R-Project.Org/.

Raud, L., Westerhausen, R., Dooley, N., and Huster, R.J. (2020). Differences in unity: the go/No-go and stop signal tasks rely on different mechanisms. Neuroimage *210*, 116582.

Ray, N.J., Brittain, J.S., Holland, P., Joundi, R.A., Stein, J.F., Aziz, T.Z., and Jenkinson, N. (2012). The role of the subthalamic nucleus in response inhibition: evidence from local field potential recordings in the human subthalamic nucleus. Neuroimage *60*, 271–278.

Reato, D., Rahman, A., Bikson, M., and Parra, L.C. (2010). Low-intensity electrical stimulation affects network dynamics by modulating population rate and spike timing. J. Neurosci. *30*, 15067–15079.

Saturnino, G.B., Antunes, A., and Thielscher, A. (2015). On the importance of electrode parameters for shaping electric field patterns generated by tdcs. Neuroimage *120*, 25–35.

Schmidt, R., Herrojo Ruiz, M., Kilavik, B.E., Lundqvist, M., Starr, P.A., and Aron, A.R. (2019). Beta oscillations in working memory, executive control of movement and thought, and sensorimotor function. J. Neurosci. *39*, 8231–8238.

Schmidt, R., Leventhal, D.K., Mallet, N., Chen, F., and Berke, J.D. (2013). Canceling actions involves A race between basal ganglia pathways. Nat. Neurosci. *16*, 1118–1124.

Slater-Hammel, A.T. (1960). Reliability, accuracy, and refractoriness of A transit reaction. Res. Q. *31*, 217–228.

Sundby, K.K., Jana, S., and Aron, A.R. (2020). Double blind disruption of right inferior frontal cortex with tms reduces right frontal beta power for action-stopping. J. Neurophysiol. *125*, 140–153.

Swann, N., Tandon, N., Canolty, R., Ellmore, T.M., Mcevoy, L.K., Dreyer, S., Disano, M., and Aron, A.R. (2009). Intracranial eeg reveals A time- and frequency-specific role for the right inferior frontal gyrus and primary motor cortex in stopping initiated responses. J. Neurosci. *29*, 12675–12685.

Swann, N.C., Cai, W., Conner, C.R., Pieters, T.A., Claffey, M.P., George, J.S., Aron, A.R., and Tandon, N. (2012). Roles for the pre-supplementary motor area and the right inferior frontal gyrus in stopping action: electrophysiological responses and functional and structural connectivity. Neuroimage *59*, 2860–2870.

Szmalec, A., Demanet, J., Vandierendonck, A., and Verbruggen, F. (2009). Investigating the role of conflict resolution in memory updating by means of the one-back choice rt task. Psychol. Res. *73*, 390–406.

Tan, J., Wansbrough, K., Williams, A.G., Nitsche, M.A., Vallence, A.M., and Fujiyama, H. (2020). The importance of model-driven approaches to set stimulation intensity for multi-channel transcranial alternating current stimulation (tacs). Brain Stimul. *13*, 1002–1004.

Thut, G., Schyns, P.G., and Gross, J. (2011). Entrainment of perceptually relevant brain oscillations by non-invasive rhythmic stimulation of the human brain. Front. Psychol. *2*, 170.

Tran, H., Shirinpour, S., and Opitz, A. (2022). Effects of transcranial alternating current stimulation on spiking activity in computational models of single neocortical neurons. Neuroimage *250*, 118953.

Van Den Wildenberg, W.P., Van Boxtel, G.J., and Van Der Molen, M.W. (2003). The duration of response inhibition in the stop-signal paradigm varies with response force. Acta Psychol. (Amst) *114*, 115–129.

Verbruggen, F., Aron, A.R., Band, G.P., Beste, C., Bissett, P.G., Brockett, A.T., Brown, J.W., Chamberlain, S.R., Chambers, C.D., Colonius, H., et al. (2019). A consensus guide to capturing the ability to inhibit actions and impulsive behaviors in the stop-signal task. Elife *8*, e46323.

Voroslakos, M., Takeuchi, Y., Brinyiczki, K., Zombori, T., Oliva, A., Fernandez-Ruiz, A., Kozak, G., Kincses, Z.T., Ivanyi, B., Buzsaki, G., and Berenyi, A. (2018). Direct effects of transcranial electric stimulation on brain circuits in rats and humans. Nat. Commun. *9*, 483.

Vossen, A., Gross, J., and Thut, G. (2015). Alpha power increase after transcranial alternating current stimulation at alpha frequency (Alpha-Tacs) reflects plastic changes rather than entrainment. Brain Stimul. *8*, 499–508.

Wach, C., Krause, V., Moliadze, V., Paulus, W., Schnitzler, A., and Pollok, B. (2013). The effect of 10 Hz transcranial alternating current stimulation (tacs) on corticomuscular coherence. Front. Hum. Neurosci. *7*, 511.

Wagner, J., Wessel, J.R., Ghahremani, A., and Aron, A.R. (2018). Establishing A right frontal beta signature for stopping action in scalp eeg: implications for testing inhibitory control in other task contexts. J. Cogn. Neurosci. *30*, 107–118.

Wessel, J.R. (2020). Beta-bursts reveal the trial-to-trial dynamics of movement initiation and cancellation. J. Neurosci. *40*, 411–423.

Wessel, J.R., Conner, C.R., Aron, A.R., and Tandon, N. (2013). Chronometric electrical stimulation of right inferior frontal cortex increases motor braking. J. Neurosci. *33*, 19611–19619.

Wessel, J.R., Ghahremani, A., Udupa, K., Saha, U., Kalia, S.K., Hodaie, M., Lozano, A.M., Aron, A.R., and Chen, R. (2016). Stop-related subthalamic beta activity indexes global motor suppression in Parkinson's disease. Mov. Disord. *31*, 1846–1853.

Woods, A.J., Antal, A., Bikson, M., Boggio, P.S., Brunoni, A.R., Celnik, P., Cohen, L.G., Fregni, F., Herrmann, C.S., Kappenman, E.S., et al. (2016). A technical guide to tdcs, and related non-invasive brain stimulation tools. Clin. Neurophysiol. *127*, 1031–1048.

STAR★METHODS

KEY RESOURCES TABLE

REAGENT or RESOURCE	SOURCE	IDENTIFIER
Deposited data		
Raw data and participant information	This paper	https://doi.org/10.34894/VWEXJE
Software and algorithms		
LabView	http://www.ni.com/labview/	RRID:SCR_014325
Net Station EEG Software	http://www.egi.com/research-division-geodesic-system-components/eeg-software	RRID:SCR_002453
MATLAB 2016a	http://www.mathworks.com/products/matlab/	RRID:SCR_001622
FieldTrip	http://www.fieldtriptoolbox.org	RRID:SCR_004849
R Project for Statistical Computing	http://www.r-project.org/	RRID:SCR_001905

RESOURCE AVAILABILITY

Lead contact

Further information and requests for resources should be directed to and will be fulfilled by the lead contact, Inge Leunissen (inge.leunissen@maastrichtuniversity.nl).

Materials availability

There are no newly generated materials.

Data and code availability

- De-identified raw data has been deposited at the DataverseNL repository: https://doi.org/10.34894/VWEXJE and is publicly available as of the date of publication.
- All original code has been deposited at the DataverseNL repository: https://doi.org/10.34894/VWEXJE and is publicly available as of the date of publication.
- Any additional information required to reanalyze the data reported in this paper is available from the lead contact upon request.

EXPERIMENTAL MODEL AND SUBJECT DETAILS

Thirty-six right-handed (laterality quotient range 33–100, mean 90.5 (Oldfield, 1971)) healthy volunteers (age range 19–28years, mean 22.5years, 15 male) were included in this study. Standard screening verified that there were no contraindications to non-invasive brain stimulation (Woods et al., 2016; Bikson et al., 2009). All procedures were approved by the local ethical committee and written informed consent was obtained from all participants.

METHOD DETAILS

Experimental design

Participants underwent two tACS-EEG sessions in which they received either 20Hz (beta) or 70Hz (gamma) stimulation during the performance of a stop-signal task. The stimulation frequency order was counterbalanced across participants, and sessions took place at least 48h apart (range 2–55 days, mean 10 days). Data acquisition in each session started with 5 min of resting EEG with eyes open while fixating on a white cross on a black background (pre-EEG), and also ended with 3 min of resting EEG (post-EEG). The level of discomfort was assessed after each session according to a Visual Analogue Scale (VAS) of 10cm length without numerical indication, extremes constituted 'absolutely no discomfort/pain' and 'worst discomfort/pain ever'. The point on the scale marked by the participant was subsequently converted into a score ranging from 1-10 (Huskisson, 1974). Similarly, participants evaluated their perceived level of fatigue with a

VAS (ranging from 'absolutely not tired' to 'maximally tired/exhausted') at the beginning and end of each experimental session.

Stop-signal paradigm

Participants performed an anticipated response stop-signal task (Coxon et al., 2006; Leunissen et al., 2017; Slater-Hammel, 1960). They were comfortably seated 1m from the computer screen (refresh rate 60Hz). The visual display consisted of a vertical indicator, presented centrally on the screen, that moved from the bottom upwards on each trial (Figure 1A). A target line was situated 800ms from onset. The primary task was to stop the indicator at the target by pinching a force transducer (OMEGA Engineering, Norwalk, CT, USA) held between the index finger and thumb of the right hand (go trials). Participants were instructed to perform these go trials as accurately and consistently as possible. The response threshold was initially set to 35% of their maximal voluntary force (MVF) and lowered in steps of 5% till participants reported they could comfortably cross the threshold (range 20–35%, mean 29%) to avoid fatigue. MVF was determined as the highest force value measured during 3 maximal strength pinches of ~5s. To reinforce go task performance the color of the target line changed to green, yellow, orange or red at the end of each trial, for responses within 20, 40, 60, or >60ms of the target, respectively. In 33% of the trials the indicator stopped automatically prior to the target. When this happened, participants tried to prevent pressing the sensor (stop trials, Figure 1A). Separate staircasing algorithms were used for stimulated and non-stimulated trials to ensure convergence to 50% success on stop trials in each condition. The initial stop time was set at 250ms from the target and was adjusted in steps of 25ms. The indicator was reset to empty after 1s. The inter-trial interval was 4.5s.

The force signal was sampled at 1000Hz on each trial from the moment that the indicator started filling. Response times were recorded as the time between indicator fill onset and the moment the force signal first exceeded the threshold. Stop trials were classified as failed stop trials if the force produced exceeded the response threshold. If the force remained below the threshold, the trial was classified as a successfully inhibited (Figure 1B). Participants practiced the task by performing 20 go trials, followed by 20 trials in which go and stop trials were mixed. Participants completed six concurrent tACS-EEG task runs per session, each comprising 67 go and 34 stop trials presented in a pseudorandomized order (606 trials per session in total).

tACS-EEG procedures

EEG was recorded with an EGI 400 Geodesic system and a 128-channel HydroCel Geodesic Sensor Net (EGI, Eugene, OR, USA) at a sampling rate of 1000Hz (Net Station v5.1.2). Cz was used as physical reference during recording and impedance was kept below 50kΩ as recommended for this system. The position of the electrodes on the participants' scalps were localized with the Geodesic Photogrammetry System (GPS 2.0, EGI, Eugene, OR, USA).

20Hz (beta) and 70Hz (gamma) tACS were applied in separate sessions using an 4 × 1 HD-tACS setup (DC Stimulator Plus, NeuroConn, Ilmenau, Germany) with a stimulation intensity of 1mA (peak-to-peak amplitude). The order of the stimulation frequency was counterbalanced over participants. The target electrode (2.5cm Ø) was placed over the preSMA (FCz) (Homan et al., 1987), and the four surrounding electrodes (2cm Ø) were placed at positions F1, F2, C1 and C2 (Figure 1C). Impedance of the tACS electrodes was kept below 10kΩ (range 1.2-7kΩ, mean 3.51kΩ). tACS was applied in an event-related manner, distributed pseudo-randomly over 40% of both go and stop trials. Each stimulation train ramped up in 0.5s, 2.5s before the start of the trial and lasted a total of 4s before ramping down again (Figure 1D). Between the end and the start of the next stimulation train was an interval of 4.5s or 9s. Over one experimental session the participants received a total of 18 min of tACS.

For the first 16 participants, the classic HydroCel Geodesic Sensor Net was used in which the electrodes are encased in plastic cups covered with sponges that are soaked in electrolyte solution. To ensure good contact of the tACS electrodes a sponge soaked in the same electrolyte solution was placed under the rubber electrodes. With this set-up the tACS stimulation caused saturation of several EEG electrodes close to the stimulation site (N = ~5–10) in about 1/3 of the participants, resulting in large artefacts even during the non-stimulated periods. The remaining 20 participants were tested using HydroCel Geodesic Sensor Net 130 LTM nets, where the cups were filled with electrolyte gel (Redux®, Parker Laboratories, Fairfield, NJ, USA). The same gel was used to ensure a good contact between skin and tACS electrodes. We refrained

from putting gel in the electrodes directly on top of the tACS electrodes. The saturation problems were completely resolved with this approach.

Behavioral analysis

Force data and response times were analyzed using Matlab R2016a (Mathworks, Natick, MA, USA).

Force data & response times

Force data was filtered with a fifth-order 20Hz low pass Butterworth filter, and baseline corrected by subtracting the average force between −650 to −300ms prior to the target. Per trial we determined: (i) peak force (i.e. maximum force in that trial), (ii) peak rate of force development, and (iii) the time to peak, which is defined as the time between the first instance that the force trace exceeds 5*SD of the baseline period and the peak. On successful stop trials force production did not always exceed 5*SD of the baseline period. To quantify this and to capture possible changes in the proportion of successful stop trials with 'perfect inhibition', we calculated the proportion of successful stop trials in which force production did exceed the threshold. In addition to the average per trial type and condition, we also calculated the percent change in peak force, peak force rate, time to peak, and the proportion of successful stop trials in which the response exceeded 5*SD of the baseline period between stimulated versus non-stimulated trials.

Go response times (goRT) and response times for unsuccessful stop trials were determined relative to the target (time of response −800ms). Early responses (>400ms before the target) and go trials where there was no response were considered errors and removed from both the force and response time data. Go trials with force output more than 2.5*SD from their respective mean were defined as outliers and removed. For stop trials, the probability of responding was calculated and stop signal reaction time (SSRT) was determined via the integration method in which go omissions were replaced with the maximum RT (1000ms) (Verbruggen et al., 2019).

To gain insight into whether stimulation affected the processes underlying going and stopping, we fitted the stop accuracy and response time distributions to a dependent process model (DPM) with the Race Against Drift Diffusion toolbox (RADD v0.5.5) (Dunovan et al., 2015; Dunovan and Verstynen, 2019). The DPM assumes that the execution process (θ_e begins to accumulate after a delay (*tr*) until reaching an upper decision threshold (*a*), yielding a go response (Figure 3 of main manuscript). The dynamics of θ_e are described by the stochastic differential equation, accumulating with a mean rate of v_e (i.e., execution drift rate) and a standard deviation described by the dynamics of a white noise process (*dW*) with diffusion constant σ as follows:

$$d\theta_e = v_e dt + \sigma dW$$

In the event of a stop signal, the braking process (θ_b) is initiated at the current state of θ_e with a negative drift rate (v_b). If θ_b reaches the 0 boundary before θ_e reaches the execution boundary no response is made. The change in θ_b over time is given by:

$$d\theta_b = v_b dt + \sigma dW$$

The dependency between θ_e and θ_b in model is implemented by declaring that the intial state of θ_b is equal to the state of θ_e.

To determine if any of the model parameters (execution drift rate (v_e), braking drift rate (v_b), boundary height (*a*) or execution onset delay (*tr*)) changed during stimulation we fitted four models to the average group data, each allowing only one of the parameters to vary for the within subject factors FREQUENCY (20Hz, 70Hz), and STIMULATION CONDITION (ON, OFF). The fitting procedure was aimed at minimizing a cost function equal to the sum of the squared and weighted errors between vectors of observed and simulated response probabilities, stop accuracy and response time quantiles of correct go responses and failed stop responses (error RT). To obtain an estimate of fit reliability for each model, we restarted the fitting procedure from 20 randomly sampled sets of initial parameter values (based on 2000 sampled parameter sets). All fits were initialized from multiple starting values in steps (step size .05) to avoid biasing model selection to unfair advantages in the initial settings. Each initial set was then optimized using a basinhopping algorithm to find the region of global minimum followed by a Nelder-Mead simplex optimization for fine-tuning globally optimized parameter values. The simplex-optimized parameter estimates were then held constant, except for the designated parameter that was submitted to a second simplex

run to find the best fitting values for the four conditions. Finally, the model fits were compared in goodness-of-fit with the Akaike information criterion (AIC) and Bayesian information criterion (BIC). A difference of AIC/BIC between 3-10 is considered moderate evidence for one model over the other and >10 as strong evidence (Lee and Wagenmakers, 2014). For more details on model fitting, model code, simulation, cost function weights, and animations see Dunovan et al., 2015, 2019 (Dunovan et al., 2015; Dunovan and Verstynen, 2019) and https://www.github.com/coaxlab/radd.

Electrical field modeling

For the last 20 participants, a Philips 3T MRI scanner with a 32-channel head coil was used to acquire high resolution T1 and T2-weighted images, with and without fat suppression. T1-weighted structural images were acquired using magnetization prepared rapid gradient echo (MPRAGE; TR = 9.60ms, TE = 4.60ms, 222 sagittal slices, 0.98 × 0.98 × 1.2mm voxels). T2-weighted structural images were acquired with TR = 2500ms, TE = 203ms, 200 sagittal slices, 1.02 × 1.01 × 1mm voxels.

To simulate the electrical field expansion of the 1-by-4 electrode montage, computational modeling was performed (www.simnibs.org) using a finite element head model derived from the four T1 and T2 scans of each individual (Opitz et al., 2015). All electrodes were modeled as a 2mm thick rubber layer (conductivity 0.1S/m) with a 1mm thick layer of conductive gel underneath (conductivity of 3S/m, as stated by the manufacturer). The positions of the tACS electrodes were determined based on the localization of the EEG electrode positions of all 128 sensors and three landmarks positions (nasion, left and right preauricular). Also the positions of the connectors were explicitly modeled (modeling procedure described in detail in Saturnino et al. (2015)). A current strength of 500μA was simulated, corresponding to 1000μA peak-to-peak amplitude. Finally, the normalized predicted electric field distribution mesh of the white and gray matter volumes was converted to nifti (https://github.com/ncullen93/mesh2nifti).

To determine a dose-response relationship a ROI was created based on preSMA peak fMRI activation coordinates (contrast stop > go) in previous studies using the same paradigm (Coxon et al., 2016; Leunissen et al., 2016) (sphere with 10mm diameter centered around the coordinate [11, 10, 62] of the Montreal National Institute (MNI) space). The ROI was transformed into subject space using the inverse of the deformation fields generated by the simnibs pipeline. Average normalized predicted electric field in the resulting individual preSMA ROIs of each session were related to the percent change in force during beta and gamma stimulation using linear regression.

EEG analysis

EEG data was analyzed using the FieldTrip toolbox (Oostenveld et al., 2011). EEG during no stimulation trials was only analyzed in the last 20 participants due to the high amount of data loss in the first 16 participants (see tACS-EEG procedures). Pre- and post-tACS resting EEG recordings were available for all 36 participants. Since non-neural signals contaminate the low amplitude gamma-band activity in scalp EEG, all analyses only focus on beta-band activity (Muthukumaraswamy, 2013).

Pre- and post-tACS resting EEG measurements

Pre- and post-tACS resting EEG recordings were re-referenced to the average reference. Bad channels were rejected upon visual inspection. Subsequently, the data was band-pass filtered (1–100 Hz), and independent component analysis was used to identify and remove ocular artifacts (see Figure S1). Finally, the data was epoched in 1s segments and bad segments were rejected upon visual inspection. A fast Fourier transformation (FFT) for frequencies between 4 and 45Hz was performed on the first 100 artifact-free segments using a Hanning window and 10s zero-padding. Changes in absolute beta power from pre-to post-tACS were investigated by calculating the percent change in mean power at 13-30Hz in the averaged pre and post spectra.

To determine the individual beta peak frequency, the resulting spectra of the pre-measurement in the 20Hz stimulation session were averaged. The 1/f component was removed by fitting a linear trend (least-squares fit) to the log-transformed spectrum (Haegens et al., 2014; Nikulin and Brismar, 2006). Subsequently, a 3rd order Gaussian curve was fitted to the power spectra to estimate the individual peak frequency.

Task performance in tACS-free intervals

To capture potential differences in event-related synchronization or desynchronization (ERS/ERD) we extracted 2s before and 0.7s after the stop signal presentation. Activity during Go trials was aligned to the average stop signal presentation time. Further pre-processing followed the same steps as for the resting-state data. EEG data of one participant had to be discarded due to excessive (eye)movements, resulting in a sample of N = 18. To avoid boundary jumps caused by the filtering procedure the first and last 300ms of the epochs were discarded. Complex Fourier spectra were extracted with Morlet wavelets between 4 and 45 Hz with step size of 0.5 Hz and a fixed width of 7 cycles. The resulting absolute time-frequency spectra were averaged per condition. For visualization, the stop-locked activity was normalized by calculating the change in power with respect to the average of the frequency-specific baseline obtained between −400 to 0ms before the stop signal. The absolute time-frequency spectra were compared with a dependent-sample cluster-based permutation t-test (two-tailed, 5000 permutations, cluster alpha of 0.05). This procedure ensures correction for multiple comparisons over time and frequencies (Maris and Oostenveld, 2007).

QUANTIFICATION AND STATISTICAL ANALYSIS

All statistical analyses were performed with R version 4.0.0 (R Core Team, 2020) using packages nlme version 3.1–147 (Pinheiro et al., 2021) and multcomp version 1.4–13 (Hothorn et al., 2008).

The influence of tACS FREQUENCY (20Hz, 70Hz), SESSION (first, second), and TIME POINT (pre, post) on subjective level of stimulation-related discomfort ($VAS_{discomfort}$) and subjective level of fatigue ($VAS_{fatigue}$) were analyzed with a repeated measures ANOVA.

For the behavioral outcome measures linear mixed effects (LME) models were specified with tACS FREQUENCY (20Hz, 70Hz) and STIMULATION CONDITION (ON, OFF) as fixed factors. For force outcome measures LME models were specified with tACS FREQUENCY, STIMULATION CONDITION (ON, OFF) and TRIAL TYPE (successful stop, go) as fixed factors. For all LMEs random intercepts were modeled on subject level (restricted maximum likelihood criteria, REML). Results for LME models are given as Type III sums of squares for sequentially fitted fixed effects (F, df, p). Significant results from simultaneous pairwise post-hoc comparisons with Tukey contrasts are reported with adjusted p values for estimates of contrasts (estimated mean difference $\pm$SE, *z*-value, adjusted p_{Tukey}).

We assessed whether the percent change in force between stimulated and non-stimulated trials was significantly different from zero using a two-tailed one-sample t-test.

A one-tailed Pearson correlation was used to assess the relationship between behavior and normalized electrical field strength.

Pearson correlations were used to test for relationships between beta activity and behavior (one-tailed, 5000 permutations). The absolute time-frequency spectra were averaged over the full frequency range (13-30Hz). An FDR correction (alpha 0.05) was applied for correcting for testing multiple time points.

The percent change scores in beta power from pre-to post-stimulation were non-normally distributed (Shapiro-Wilk test $p < 0.05$). Therefore, a one-sample Wilcoxon Signed Rank Test was used to test whether the percent change in beta power was significantly different from zero. The 20 and 70Hz sessions were compared with the Wilcoxon signed-rank test.

Descriptive statistics are given as average $\pm$ standard deviation unless indicated differently.